ADVANCED MATERIALS INTERFACES
www.advmatinterfaces.de

LSPR-Enhanced Pyro-Phototronic Effect for UV Detection with an Ag–ZnO Schottky Junction Device

Jing Huang, Qi Li, Xianmao Lu, Jianping Meng, and Zhou Li**

Sensitive and rapid detection of low-power density ultraviolet (UV) light is of great significance for various applications such as space exploration, biological analysis, environmental sensors, communications, and imaging. However, the persistent photoconductivity (PPC) of photodetectors, which are based on ZnO, will cause a long decay time and make it difficult to capture weak light signals. In this work, the pyro-phototronic effect of ZnO is integrated with the localized surface plasmon resonance (LSPR) of Ag nanoparticles (NPs) to enhance the performance of ZnO-based photodetectors. The self-powered photodetector is consisted of the ZnO nanowires (ZnO NWs) and Ag NPs, which can detect 325 nm UV light with a power density of 340 nW cm^{-2} quickly and sensitively. Compared with the photodetector without Ag NPs, the performance is significantly improved. Under the 325 nm UV light with the same power density, the best responsivity, and detectivity are 8.82×10^{-5} A W^{-1} and 4.9×10^{10} Jones, respectively. And the fast response time is remarkably reduced to 8.72 ms. These results help to understand the performance of LSPR enhanced photodetectors deeply and expand the methods for preparing high-performance photodetectors.

1. Introduction

UV detection is of overriding importance because it has been widely employed in power industry, environmental monitoring, military applications, and life sciences, such as cell carcinogenesis analysis, automobile exhaust monitoring, missile tracking, fire monitoring, etc.[1–4] Generally, the performance of UV detector is strongly depended on the sensing materials, and the wide bandgap semiconductors, which include GaN, SiC, ZnO, MoS_2, InSe, etc,[5–9] are the preferred candidates owing to the high selectivity for UV light. Among them, ZnO is a prior choice for fabricating UV photodetectors at room temperature owing to the high electron mobility,[10] suitable bandgap (3.37 eV), high exciton binding energy (60 meV),[11] and low-cost preparation process with low cost.[12] Besides, the morphologies of ZnO NWs can increase the interaction area between UV light and ZnO NWs due to their high surface to volume ratio.[13] Particularly, a self-powered photodetector based on ZnO NWs was constructed by built-in potential in a p–n junction[14] or Schottky junction.[15,16]

However, the inevitable oxygen vacancy defects in ZnO[17] will cause the persistent photoconductivity (PPC) effect, which prolongs the response and recovery time.[18,19] Pyro-phototronic effect of ZnO is an effective way to shorten the response/recovery time remarkably by using pyroelectric potential generated from the light-heating effect.[20,21] The ultrafast UV sensing will be achieved by introducing light-induced pyro-phototronic effect.[22–24] Whereas the photon-heating effect was weakened gradually as the wavelength decreased to the visible range even to UV wave.[25,26] Two strategies are adopted to improve the pyroelectric current for UV light, which includes: (i) decreasing substrate temperature, and (ii) improving the photothermal conversion of UV light. The disadvantage of the first strategy is that impedes the applications of photodetector at room temperature.

When the light illuminates on the metal NPs, transient thermal power can be generated in metal NPs within 100 ps by LSPR.[27–30] The high-quality factor of Ag in the UV wavelength range leads to strong LSPR.[31] Ag NPs are widely used to enhance the light emission of ZnO due to its strong LSPR in wavelength range.[32,33] Here, we propose a strategy to enhance the photothermal conversion of UV light by LSPR of Ag NPs because of the high-quality factor of Ag NPs in UV wavelength range, and then it can raise temperature variation of ZnO NWs noticeably at the moment of turning on/off light. A self-powered photodetector based on the Schottky junction of Ag and ZnO NWs after decorating Ag NPs was

J. Huang, Q. Li, X. Lu, Z. Li
College of Chemistry and Chemical Engineering
Center on Nanoenergy Research
Guangxi University
Nanning 530004, China
J. Huang, Q. Li, X. Lu, J. Meng, Z. Li
CAS Center for Excellence in Nanoscience
Beijing Key Laboratory of Micro-Nano Energy and Sensor
Beijing Institute of Nanoenergy and Nanosystems
Chinese Academy of Sciences
Beijing 101400, China
E-mail: mengjianping@binn.cas.cn; zli@binn.cas.cn
X. Lu, J. Meng, Z. Li
School of Nanoscience and Technology
University of Chinese Academy of Sciences
Beijing 100049, China
Z. Li
Institute for Stem Cell and Regeneration
Chinese Academy of Sciences
Beijing 100101, China
The ORCID identification number(s) for the author(s) of this article can be found under https://doi.org/10.1002/admi.202200327.

DOI: 10.1002/admi.202200327

designed to detect the UV light with the low power density. Responsivity and detectivity reaches 8.82×10^{-5} A W^{-1} and 4.9×10^{10} Jones for the devices with Ag loading of 30.9 μmol. The fast response and recovery ensure the sensing process can be finished within 8.72 ms. The result in our work provides an ingenious way to develop high performance photodetector with other materials.

2. Results and Discussions

Figure 1a illustrated the schematic structure of the ZnO NWs before and after being decorated with Ag NPs. First, the ZnO NWs were grown by hydrothermal method. After that, the Ag NPs were decorated on the surface of ZnO NWs by the sputtering process (Figure 1a). The size of Ag NPs is mainly ranged

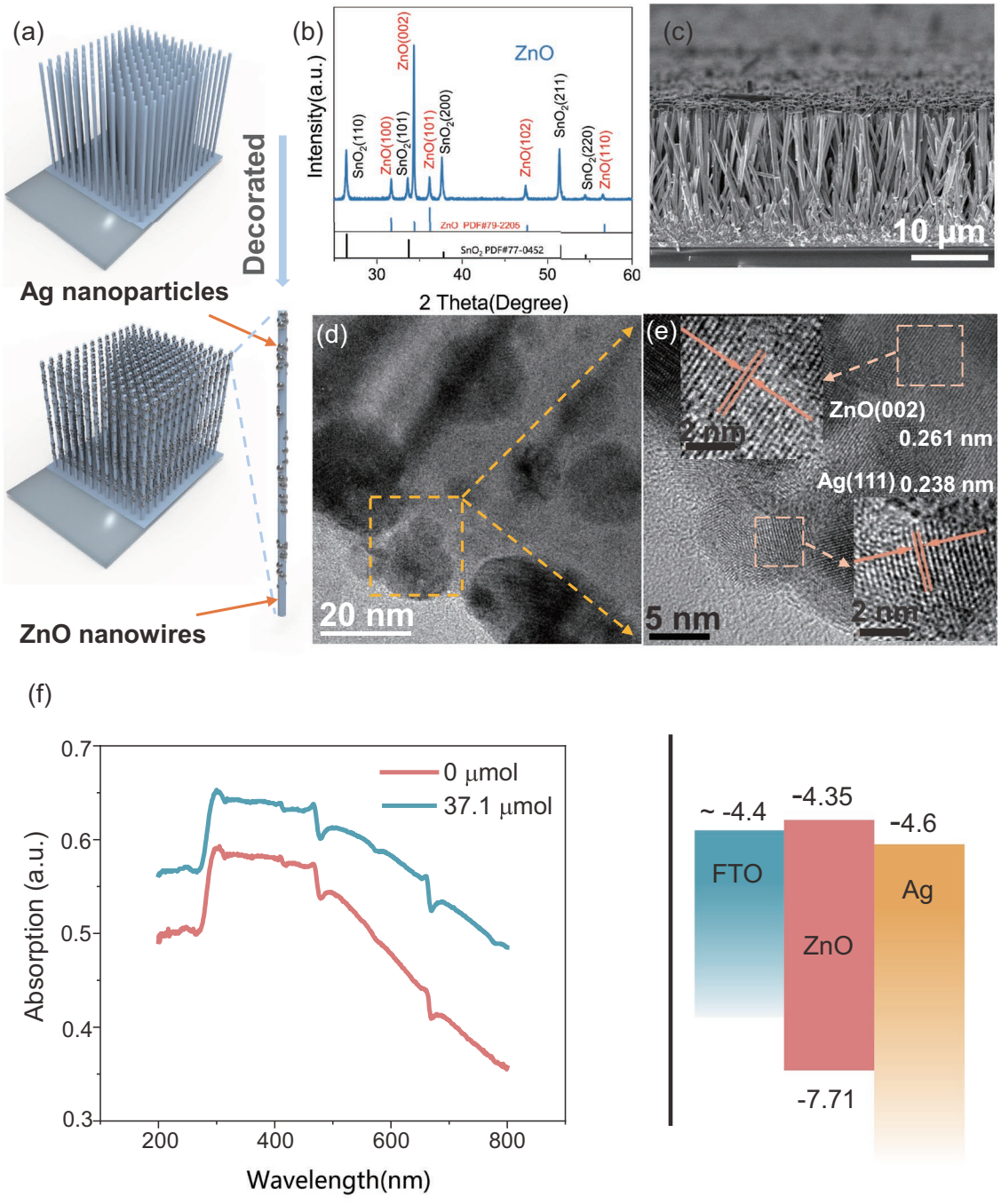

Figure 1. The structure and characterization of Ag–ZnO NWs. a) Schematic diagram of the structure of the Ag–ZnO NWs array. b) XRD pattern of ZnO NWs array without sputtering Ag NPs. c) Cross-sectional view SEM images of ZnO NWs. d,e) The TEM and HRTEM image of the ZnO NWs after being decorated with Ag NPs. f) UV absorption spectrums of ZnO NWs modified with and without Ag NPs. g) Energy band diagram of FTO, ZnO, Ag under zero bias.

from 10 to 20 nm (Figure S1, Supporting Information). The noticeable diffraction peaks from (002) crystal plane of ZnO can be observed from XRD patterns, which confirms that ZnO NWs were preferentially grown along as *c*-axis (Figure 1b).[34,35] A further proof can be found from the selected area electron diffraction (SEAD) (Figure S2d, Supporting Information). And the peaks at 31.765°, 34.418°, 36.250°, 47.534°, 56.589° respectively represented the diffraction of crystal plane from SnO_2 of FTO substrate (PDF# 77–0452).[36,37] From the SEM image (Figure 1c), we can clearly see that the uniform ZnO NWs array grow on the FTO vertically. The height of a single ZnO nanowire was about 15 µm, and the diameter was about 500 nm. After decorating Ag NPs on the surface of ZnO NWs, the microstructure was analyzed by using TEM (Figure 1d). Ag NPs can be found clearly from the TEM image in Figure 1d. A further proof can be confirmed from the measurement of crystal plane in HRTEM (Figure 1e), which corresponded to the planes of ZnO (002) planes (0.261 nm) and Ag (111) planes (0.238 nm).[38] The Zn element and O element mainly distributed in the core region from energy dispersive spectroscopy (EDS) (Figure S2a–c, Supporting Information), while Ag element distribute on the surface of the nanowire mostly. The absorption of ZnO NWs before and after being decorated with Ag NPs showed high absorption in UV range compared with the absorption in visible range (Figure 1f; Figure S3, Supporting Information). Besides, the absorption of ZnO NWs after being decorated with Ag NPs of 37.1 µmol was enhanced in the UV–vis range (As shown the light blue line in Figure 1f). It indicated Ag NPs can increase the absorption, which was beneficial to increase the temperature variation by improving photothermal conversion efficiency. The energy band diagram of the related materials under zero bias was shown in Figure 1g. Schottky junction was formed owing to the high work function of Ag (4.64 eV) and low electron affinity of ZnO (4.35 eV). The approximate conductive band of FTO and ZnO makes the formation of Ohmic contact. The nonlinear nonsymmetrical *I–V* curves of samples confirmed the Schottky contact between Ag and ZnO NWs and asymmetric structure at both ends (Figure S4, Supporting Information).

I–t curves were recorded to characterize the performance of photoresponse under the illumination of 325 nm light with different power densities. Under the illumination of 325 nm light with the power density of 340 nW cm^{-2}, the original device showed a weak response (**Figure 2**a). While the photoresponse was enhanced significantly as the increase of loading amount of Ag NPs. The obvious feature of photoresponse can be noticed from the *I–t* curves of devices after being decorated with Ag NPs of 30.9 µmol (Figure 2a). Then, the photoresponse current decreased. The above results proved that the transient thermal power generated by LSPR of Ag NPs can improve the performance of photoresponse by enhanced pyro-phototronic effect. Whereas abundant Ag NPs will lead to aggregate and grow into the big particles, which resulted in the enhancement of scattering effect remarkably owing to the increase of scattering cross-section. At last, it deteriorated the performance of photothermal conversion. The low dark current of devices is owing to the suppression from Schottky barrier formed between Ag and ZnO NWs (Figure S5, Supporting Information), which

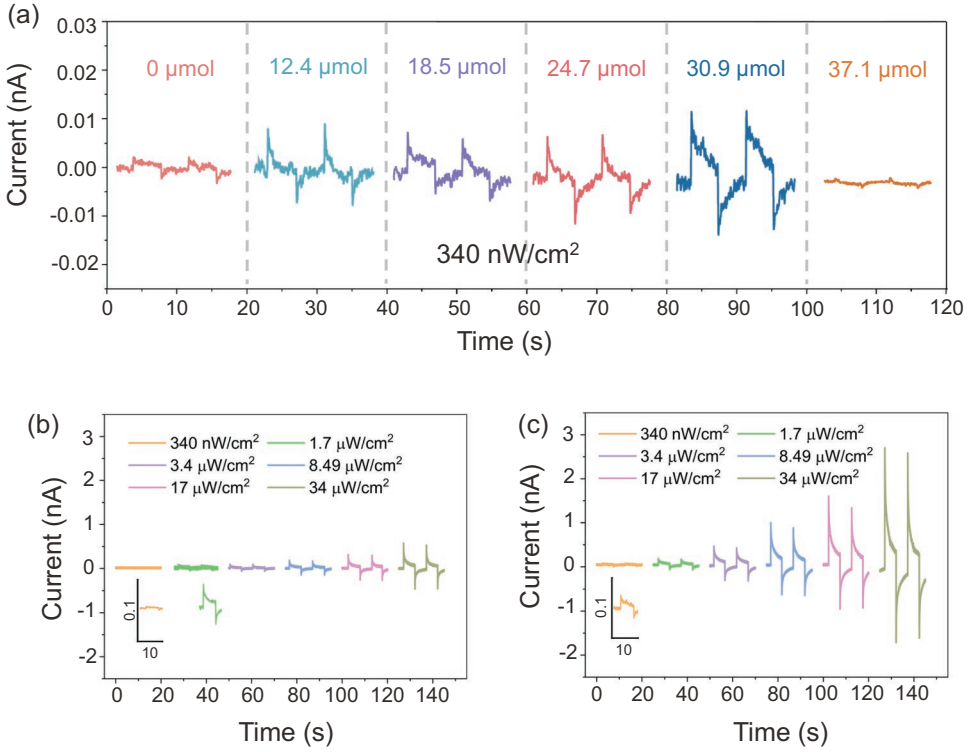

Figure 2. Photoresponse of Ag–ZnO photodetectors. a) Under the low power density of 340 nw cm^{-2}, the *I–t* characteristic curves of Ag–ZnO photodetectors with different loadings of Ag NPs from 0 to 37.1 µmol at zero bias. The *I–t* characteristic curves of Ag–ZnO photodetectors with Ag NPs loadings of b) 0 µmol and c) 30.9 µmol when the laser power density increased from 340 nW cm^{-2} to 34 µW cm^{-2} under 325 nm.

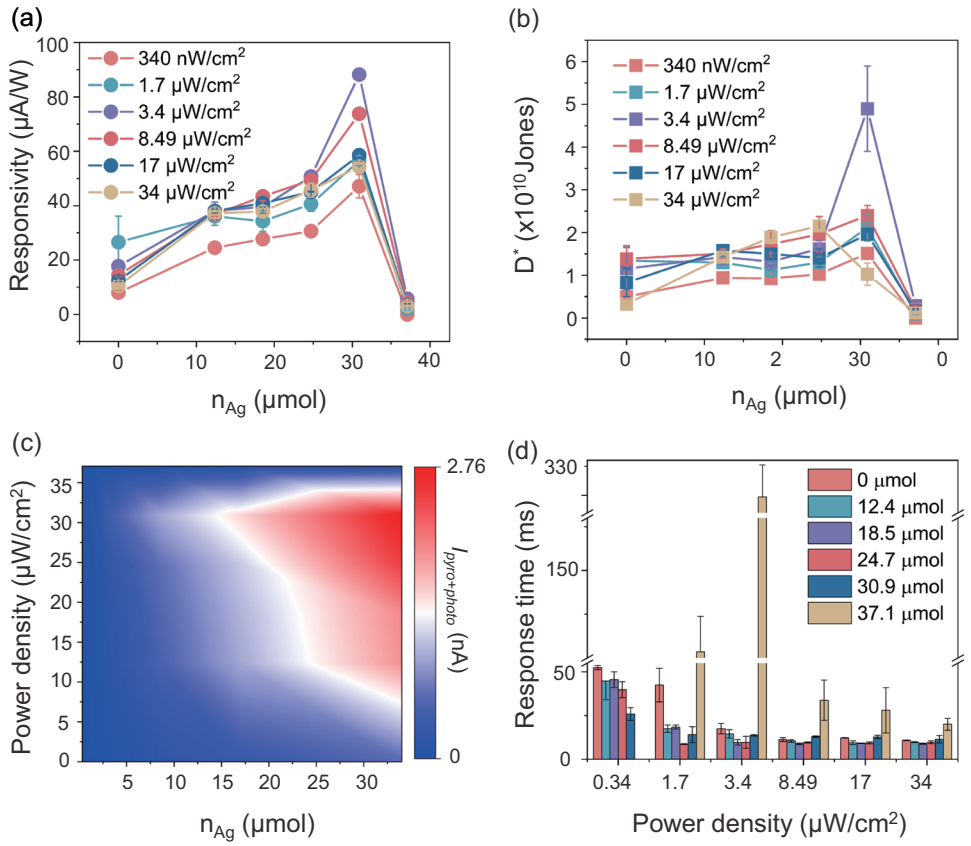

Figure 3. The LSPR-enhanced performance of Ag–ZnO photodetectors on UV detection. a) Under different power densities (325 nm), the responsivity of the Ag–ZnO photodetectors changed as the loading of Ag NPs increases ($n = 3$). b) The detectivity of the Ag–ZnO photodetectors varied as the loading of Ag NPs increased under various power density ($n = 3$). c) The $I_{pyro+photo}$ of the Ag–ZnO photodetectors with various loadings of Ag NPs under different power density. d) Response time of UV detectors with different loadings of Ag NPs under various power densities ($n = 3$).

is beneficial for the responsivity and detectivity. The comparation of photoresponse between the photodetectors without Ag NPs and the photodetectors with a loading Ag NPs of 30.9 μmol was respectively shown in Figure 2b,c under the illumination of 325 nm light with the power density ranged from 340 nW cm^{-2} to 34 μW cm^{-2}. It was found that the photoresponse current was improved monotonically as the increase of power density. At various power densities, the photoresponse current of the photodetectors after being decorated with Ag NPs showed significant improvement of over 200% compared with the corresponding performance of the original devices (Figure 2b,c), which indicated that the LSPR effect caused by Ag NPs can enhance the performance of the photodetectors significantly.

As the important parameters to evaluate the performance of the photodetectors,[39] the responsivity (R), detectivity (D^*), and response/recovery time of photodetectors after decorated with Ag NPs were calculated according to I–t curve (Figures S6 and S7, Supporting Information). The response time is defined as the time from 10% to 90% of the maximum current as light turned on, and the recovery time is defined as the falling time from 90% to 10% of the maximum photocurrent as light turn off. From **Figure 3**a, we can find that the responsivity initially raised as the increase of loading amount of Ag NPs. The maximum of responsivity can reach 88.2 μA W^{-1} for the photodetector after decorating Ag NPs of 30.9 μmol. Then it decreased. The phenomenon that the responsivity of photodetector decreased sharply after decorating Ag NPs of 37.1 μmol was owing to the increase of scattering effect caused by the aggregation of Ag NPs. The reflectance and transmittance spectra of Ag–ZnO photodetectors with 30.9 and 37.1 μmol loadings of Ag NPs was measured, respectively (Figure S8, Supporting Information), and the corresponding light harvesting efficiency (LHE) was calculated as LHE = 1 – transmittance% – reflectance%. LHE of Ag–ZnO photodetectors decorating Ag NPs of 30.9 μmol was higher than that of Ag–ZnO photodetectors decorating Ag NPs of 37.1 μmol, which indicated the absorption of photodetector after decorating Ag NPs 37.1 μmol is decreased owing to the increase of scattering effect from big Ag NPs. The abundant Ag NPs on the surface of ZnO NWs resulted in the aggregation of Ag NPs into the big particles, which led to enhance scattering noticeably with a weak increase of absorption. The detectivity of photodetector after decorating Ag NPs of 30.9 μmol exhibits the significantly enhancement comparing with the original device. The maximum value of detectivity is 4.9×10^{10} Jones for photodetector after decorating Ag NPs of 30.9 μmol at the power density of 3.4 μW cm^{-2} (Figure 3b). We have compared performance of the LSPR enhanced ZnO-Ag photodetectors with other ZnO-based photodetectors in **Table 1**. From the table, our devices exhibit the advantage in detecting the weak UV light (325 nm). The detectivity can attain

Table 1. Comparison of the different ZnO-based devices.

Device	Wavelength [nm]	τ_r/τ_d	R [mA W^{-1}]	D^* [Jones]	Power density	Bias [V]	Ref.
Au/ZnO	365	15 µs	4.68×10^3	8.18×10^{11}	0.5 mW cm^{-2}	1.5	[40]
ZnO:Ga/Si	370	79/132 µs	250	2.3×10^{12}	0.5 mW cm^{-2}	0	[41]
ZnO:Ga/GaN	370	0.044 s	>5	/	0.11 mW cm^{-2}	0	[42]
Si/SnO_x/ZnO	405	3/2 µs	36.7	1.5×10^{11}	36.3 mW cm^{-2}	0	[43]
	515	3/2 µs	53	2.0×10^{11}			
	650	2/1 µs	64.1	2.4×10^{11}			
V_2O_5/ZnO	365	4/16 µs	36.34	6.04×10^{14}	4 mW cm^{-2}	0	[44]
NiO/ZnO	400	24/212 ms	3.85×10^3	9.6×10^{13}	80 µW cm^{-2}	5	[45]
ZnO/GaN	352	0.1 s	0.34×10^3	4.25×10^{10}	5–20 mW cm^{-2}	0	[46]
ZnO/Si	1064	15/21 µs	0.16×10^3	8.8×10^{11}	26 mW cm^{-2}	2	[47]
Cl:ZnO/PEDOT:PSS	365	28/32 ms	2.33	1.54×10^{10}	0.3 mW cm^{-2}	0	[48]
ZnO/Spiro-MeOTAD	365	0.16/0.2 s	0.8	4.2×10^9	1 mW cm^{-2}	0	[49]
Ag–ZnO	325	25.87 ms	0.047	1.51×10^{10}	340 nW cm^{-2}	0	This work

1.51×10^{10} Jones for the 325 nm light with the low power density of 340 nW cm^{-2}. The corresponding 2D mapping of the $I_{pyro+photo}$ as functions of the power density and the loadings of Ag NPs was plotted in Figure 3c, indicating larger $I_{pyro+photo}$ could be obtained under stronger power density and appropriate loadings of Ag NPs, with a maximum value of 2.76 nA achieved under 325 nm 34 µW cm^{-2} UV illumination and Ag NPs of 30.9 µmol. This further verified that the LSPR effect from the appropriate amount of Ag NPs on the surface of ZnO NWs can significantly improve the responsivity of the photodetectors. The response time measured from the *I*–*t* curves was shown in Figure 3d. When applied a power density of 1.7 µW cm^{-2}, the response time of photodetectors after decorating Ag NPs of 24.7 and 30.9 µmol was only ≈8.72 and ≈14.17 ms, respectively. Response time was shortened noticeably. The faster response of the photodetectors after decorated with Ag NPs was attributed to the enhanced pyroelectric potential because of the huge transient thermal power generated by LSPR effect of Ag NPs.

The working mechanism of the Ag–ZnO photodetectors was clearly shown in **Figure 4**a–d. It can be divided into four stages. Figure 4a displayed the energy band diagram of the Ag–ZnO Schottky junction at dark condition. The Schottky junction was formed, and the valance band and conduction band were bent upward. Once the 325 nm light illuminated on the surface of ZnO NWs, the ephemeral pyroelectric potential generated along the *c*-axis, which made the energy band bent downward. The Schottky barrier height was decreased. The spike current was emerged (Figure 4b). At the same time, LSPR caused by Ag NPs on the surface of ZnO NWs boosted the temperature variation at the moment of light illumination, which enhanced the pyroelectric current for the weak light. At the same time, the photogenerated electron–hole pairs will be separated by built-in potential, the self-powered detection was achieved. The *I*–*t* curve was composed of spike current and pyroelectric current. In addition, the plasmonic hot electrons will be beneficial to the increase of photocurrent of Ag–ZnO photodetectors.[50–52] Moreover, the positive charge generated within ZnO NWs at the interface of Ag–ZnO caused the energy band bent downwards, which led to a reduction in the barrier height of the Ag–ZnO Schottky junction. And the photoresponse current was detected because more electron–hole pairs can flow across the Ag–ZnO interface. The pyroelectric potential was disappeared because of the vanishment of temperature variation even if the 325 nm light illuminated all the time. The change of energy band was disappeared (Figure 4c). The photoresponse current dropped sharply and reached a plateau at last. Once the light was turned off, the negative polarization charges generated by reverse pyroelectric potential impelled that the energy band bent upward, then, the Schottky barrier height was increased (Figure 4d). The reverse spike current emerged. Immediately, the current recovered into the dark current.

3. Conclusion

To sum up, we designed a self-powered photodetector based on the Ag–ZnO Schottky junction which can be used to detect UV light with low power density. The photodetector not only coupled the photovoltaic effect and the pyroelectric effect of the ZnO NW itself, but also bound the LSPR effect caused by the Ag NPs locating on the surface of the nanowires. The LSPR-enhanced pyro-phototronic effect will enhance the detection performance of Ag–ZnO photodetectors. Under the illumination of 325 nm light with the power density of 3.4 µW cm^{-2}, the responsivity and detectivity of the photodetectors after decorated with Ag NPs of 30.9 µmol exhibited 8.82×10^{-5} A W^{-1} and 4.9×10^{10} Jones, respectively. While the photodetector without Ag NPs showed responsivity of 1.76×10^{-5} A W^{-1} and detectivity of 1.15×10^{10} Jones. Besides, under the 325 nm light illumination of 1.7 µW cm^{-2}, the response time of photodetectors without Ag NPs displayed the response time of 42.44 ms, while the Ag–ZnO photodetectors with 24.7 µmol loadings of Ag NPs showed a faster response time of 8.72 ms, which was 4.9 times shorter than the former. The comparison of the above results further proved that the combination of photovoltaic effect, pyroelectric effect, and LSPR effect can greatly improve

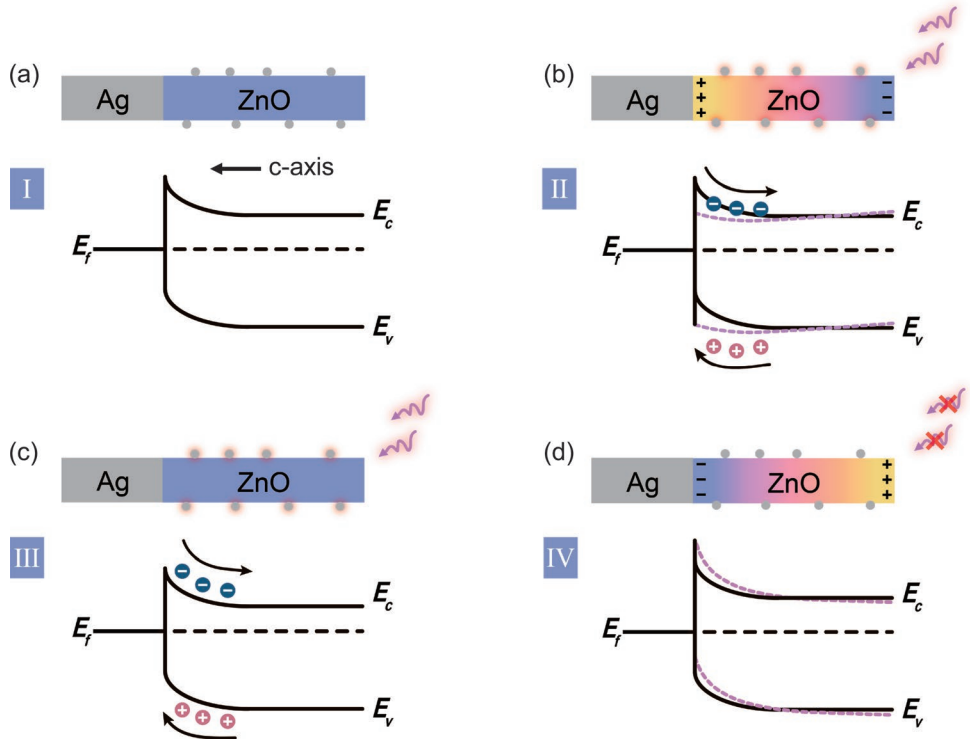

Figure 4. Working mechanism diagram of Ag–ZnO photodetectors. a) Band diagram of Ag–ZnO Schottky junction without light. b) Band diagram of Ag–ZnO Schottky junction at the moment of turn-on. c) After a period of light illumination, the change of band diagram disappeared. d) Band diagram of Ag–ZnO Schottky junction once the light turned off.

the detection performance of photodetectors which made them possess potential value in the fields of national defense security, power industry, environmental monitoring, and life sciences. Moreover, the basic principles found in this work can easily be extended to the other pyroelectric photoelectric devices based on varied semiconductor materials, laying the foundation for the design of high-performance photodetectors based on other nanomaterial systems, and broadening the application fields.

4. Experimental Section

The Fabrication of Ag–ZnO NWs Arrays and Device: The F-doped tin oxide (FTO) glasses with the size of 2×2 cm^2 were used as substrates. Before the deposition, the FTO glasses were ultrasonically cleaned with acetone and ethanol at room temperature. Then, the seed layer of ZnO with the thickness of 100 nm was deposited by radio frequency (RF) magnetron sputtering. A hydrothermal method was used to grow ZnO NWs through immersing into the solution, which was consisted of 20×10^{-3} M zinc nitrate ($Zn(NO_3)_2{\cdot}6H_2O$), 20×10^{-3} M hexamethylenetetramine (HMTA), and 5 vol % ammonium hydroxide (NH_4OH). After that, the reaction was conducted at the 90 °C for 8 h. Then the Ag NPs was deposited on the surface of ZnO NWs by DC magnetron sputtering. The loading amount of Ag NPs can be controlled by regulating the sputtering time ranged from 0 to 60 s. By depositing Ag NPs on Si plates for ten minutes, the loading amount of Ag NPs of per area in unit time was obtained. When the sputtering time increased from 0 to 60 s, the loading amount of Ag NPs was 0 µmol (0 s), 12.4 µmol (20 s), 18.5 µmol (30 s), 24.7 µmol (40 s), 30.9 µmol (50 s), and 37.1 µmol (60 s), respectively. At last, the silver paste was used to fix the wires on the ZnO NWs and FTO, respectively, as the top and bottom electrodes.

Material Characterization: The phase structures of ZnO NWs were analyzed by X-ray diffractometer (XRD) (PANalytical X'Pert) with Cu K_α source, and the microscopic morphology was observed by the scanning electron microscope (SEM) (Nova Nano SEM 450). Also, the morphology of the ZnO NWs after decorated with Ag NPs was carried out through the transmission electron microscope (TEM) and high-resolution transmission electron microscope (HRTEM) (JEM-2100F), while the element dispersion of the NWs was characterized by energy dispersive spectroscopy (EDS). The absorbance spectra were obtained by using the UV–vis–NIR spectrophotometer (SHIMADZU UV3600) under the room temperature.

Performance Measurements of the UV Photodetector: The light source was the monochromatic 325 nm lasers (KIMMON IK330IR-G), and the light power density was adjusted by continuously variable filter. Then, a digital power meters (Thorlab PM100D) was used to measure power density. The *I–V* characteristics of device was characterized by the semiconductor analysis system (Keithley 4200) and the *I–t* characteristics was recorded by the Tektronix oscilloscope (type: HD06104) and Keithley 6517 system.

Supporting Information

Supporting Information is available from the Wiley Online Library or from the author.

Acknowledgements

The authors are thankful for the support provided by the Natural Science Foundation of Beijing Municipality (2214083, JQ20038, L212010), the National Natural Science Foundation of China (52002027, T2125003, 61875015), the Strategic Priority Research Program of the Chinese Academy of Sciences (XDA16021101).

Conflict of Interest

The authors declare no conflict of interest.

Data Availability Statement

Research data are not shared.

Keywords

localized surface plasmon resonance, photodetectors, pyro-phototronic effect, Schottky junction

Received: February 10, 2022
Revised: May 8, 2022
Published online:

[1] Z. Jin, L. Gao, Q. Zhou, J. Wang, *Sci. Rep.* **2014**, *4*, 4268.
[2] H. Liu, N. Gao, M. Liao, X. Fang, *Sci. Rep.* **2015**, *5*, 7716.
[3] Z. Zheng, F. Zhuge, Y. Wang, J. Zhang, L. Gan, X. Zhou, H. Li, T. Zhai, *Adv. Funct. Mater.* **2017**, *27*, 1703115.
[4] M. Qiu, P. Sun, Y. Liu, Q. Huang, C. Zhao, Z. Li, W. Mai, *Adv. Mater. Technol.* **2018**, *3*, 1700288.
[5] Q. Li, J. Meng, J. Huang, Z. Li, *Adv. Funct. Mater.* **2022**, *32*, 2108903.
[6] F. Gao, H. Chen, W. Feng, Y. Hu, H. Shang, B. Xu, J. Zhang, C. Y. Xu, P. Hu, *Adv. Funct. Mater.* **2021**, *31*, 2104359.
[7] M. Dai, H. Chen, F. Wang, M. Long, H. Shang, Y. Hu, W. Li, C. Ge, J. Zhang, T. Zhai, Y. Fu, P. Hu, *ACS Nano* **2020**, *14*, 9098.
[8] J. Jiang, Q. Wang, B. Wang, J. Dong, Z. Li, X. Li, Y. Zi, S. Li, X. Wang, *Nano Energy* **2019**, *59*, 545.
[9] X. Wang, W. Peng, R. Yu, H. Zou, Y. Dai, Y. Zi, C. Wu, S. Li, Z. L. Wang, *Nano Lett.* **2017**, *17*, 3718.
[10] Y. Ji, L. Wu, Y. Liu, Y. Yang, *Nano Energy* **2021**, *89*, 106449.
[11] M. H. Huang, S. Mao, H. Feick, H. Q. Yan, Y. Y. Wu, H. Kind, E. Weber, R. Russo, P. D. Yang, *Science* **2001**, *292*, 1897.
[12] J. Meng, H. Li, L. Zhao, J. Lu, C. Pan, Y. Zhang, Z. Li, *Nano Lett.* **2020**, *20*, 4968.
[13] Z. Zhang, Z. Kang, Q. Liao, X. Zhang, Y. Zhang, *Chin. Phys. B* **2017**, *26*, 118102.
[14] Y. Zhang, M. Hu, Z. Wang, *Nano Energy* **2020**, *71*, 104630.
[15] Y. Wang, L. Zhu, Y. Feng, Z. Wang, Z. L. Wang, *Adv. Funct. Mater.* **2019**, *29*, 1807111.
[16] S. Liu, Q. Liao, S. Lu, Z. Zhang, G. Zhang, Y. Zhang, *Adv. Funct. Mater.* **2016**, *26*, 1347.
[17] J. Meng, Q. Li, J. Huang, Z. Li, *Nanoscale* **2021**, *13*, 17101.
[18] Y. K. Su, S. M. Peng, L. W. Ji, C. Z. Wu, W. B. Cheng, C. H. Liu, *Langmuir* **2010**, *26*, 603.
[19] S. Jeon, S.-E. Ahn, I. Song, C. J. Kim, U. I. Chung, E. Lee, I. Yoo, A. Nathan, S. Lee, K. Ghaffarzadeh, J. Robertson, K. Kim, *Nat. Mater.* **2015**, *14*, 452.
[20] J. Meng, Z. Li, *Adv. Mater.* **2020**, *32*, 2000130.
[21] Z. Wang, R. Yu, C. Pan, Z. Li, J. Yang, F. Yi, Z. L. Wang, *Nat. Commun.* **2015**, *6*, 8401.
[22] Z. Wang, R. Yu, X. Wang, W. Wu, Z. L. Wang, *Adv. Mater.* **2016**, *28*, 6880.
[23] L. Wang, H. Xue, M. Zhu, Y. Gao, Z. Wang, *Nano Energy* **2022**, *97*, 107163.
[24] D. Zhang, H. Wu, C. R. Bowen, Y. Yang, *Small* **2021**, *17*, 2103960.
[25] J. Meng, Q. Li, J. Huang, C. Pana, Z. Li, *Nano Today* **2022**, *43*, 101399.
[26] W. Ouyang, J. Chen, Z. Shi, X. Fang, *Appl. Phys. Rev.* **2021**, *8*, 031315.
[27] J. W. Stewart, J. H. Vella, W. Li, S. Fan, M. H. Mikkelsen, *Nat. Mater.* **2020**, *19*, 158.
[28] B. Ciraulo, J. Garcia-Guirado, I. de Miguel, J. Ortega Arroyo, R. Quidant, *Nat. Commun.* **2021**, *12*, 2001.
[29] X. Chen, Y. Chen, M. Yan, M. Qiu, *ACS Nano* **2012**, *6*, 2550.
[30] G. Yu, J. Qian, P. Zhang, B. Zhang, W. Zhang, W. Yan, G. Liu, *Nat. Commun.* **2019**, *10*, 4912.
[31] M. Rycenga, C. M. Cobley, J. Zeng, W. Li, C. H. Moran, Q. Zhang, D. Qin, Y. Xia, *Chem. Rev.* **2011**, *111*, 3669.
[32] W. Z. Liu, H. Y. Xu, C. L. Wang, L. X. Zhang, C. Zhang, S. Y. Sun, J. G. Ma, X. T. Zhang, J. N. Wang, Y. C. Liu, *Nanoscale* **2013**, *5*, 8634.
[33] P. Cheng, D. Li, Z. Yuan, P. Chen, D. Yang, *Appl. Phys. Lett.* **2008**, *92*, 041119.
[34] A. K. Zak, W. H. A. Majid, M. E. Abrishami, R. Yousefi, *Solid State Sci.* **2011**, *13*, 251.
[35] Y. K. Tseng, C. J. Huang, H. M. Cheng, I. N. Lin, K. S. Liu, I. C. Chen, *Adv. Funct. Mater.* **2003**, *13*, 811.
[36] N. G. Park, G. Schlichthorl, J. van de Lagemaat, H. M. Cheong, A. Mascarenhas, A. J. Frank, *J. Phys. Chem. B* **1999**, *103*, 3308.
[37] J. Q. Hu, Y. Bando, Q. L. Liu, D. Golberg, *Adv. Funct. Mater.* **2003**, *13*, 493.
[38] Y. Ning, Z. M. Zhang, F. Teng, X. S. Fang, *Small* **2018**, *14*, 1703754.
[39] D. You, C. Xu, W. Zhang, J. Zhao, F. Qin, Z. Shi, *Nano Energy* **2019**, *62*, 310.
[40] S. Podder, B. Basumatary, D. Gogoi, J. Bora, A. R. Pal, *Appl. Surf. Sci.* **2021**, *537*, 147893.
[41] R. Dai, Y. Liu, J. Wu, P. Wan, X. Zhu, C. Kan, M. Jiang, *Opt. Express* **2021**, *29*, 30244.
[42] P. Wan, M. Jiang, T. Xu, Y. Liu, X. Fang, C. Kan, *Adv. Opt. Mater.* **2021**, *10*, 2101851.
[43] J. P. B. Silva, E. M. F. Vieira, K. Gwozdz, A. Kaimc, L. M. Goncalves, J. L. MacManus-Driscoll, R. L. Z. Hoye, M. Pereira, *Nano Energy* **2021**, *89*, 106347.
[44] M. Kumar, M. Patel, T. T. Nguyen, J. Kim, J. Yi, *Nanoscale* **2018**, *10*, 6928.
[45] M. Patel, H. S. Kim, J. Kim, *Adv. Electron. Mater.* **2015**, *1*, 1500232.
[46] D. J. Lee, S. R. Ryu, G. M. Kumar, H. D. Cho, D. Y. Kim, P. Ilanchezhiyan, *Appl. Surf. Sci.* **2021**, *558*, 149896.
[47] L. Chen, B. Wang, J. Dong, F. Gao, H. Zheng, M. He, X. Wang, *Nano Energy* **2020**, *78*, 105260.
[48] B. B. Deka, M. S. Naidu, S. Nandi, A. Misra, *Nanoscale* **2018**, *10*, 3451.
[49] Y. Shen, X. Yan, H. Si, P. Lin, Y. Liu, Y. Sun, Y. Zhang, *ACS Appl. Mater. Interfaces* **2016**, *8*, 6137.
[50] H. Tang, C. J. Chen, Z. Huang, J. Bright, G. Meng, R. S. Liu, N. Wu, *Chem. Phys.* **2020**, *152*, 220901.
[51] Q. Li, J. Huang, J. Meng, Z. Li, *Adv. Opt. Mater.* **2022**, *10*, 2102468.
[52] Q. Li, Z. Li, J. Meng, *Int. J. Optomechatronics* **2022**, *16*, 1.